RSC Advances

PAPER

View Article Online
View Journal | View Issue

Cite this: *RSC Adv.*, 2017, **7**, 25582

Effect of an external electric field on the electronic properties of SnS_2/PbI_2 van der Waals heterostructures

Yaqiang Ma,[a] Xu Zhao,*[a] Mengmeng Niu,[a] Xianqi Dai,*[ab] Wei Li,[a] Yi Li,[a] Mingyu Zhao,[a] Tianxing Wang[a] and Yanan Tang[b]

Received 15th February 2017
Accepted 3rd May 2017

DOI: 10.1039/c7ra01920c

rsc.li/rsc-advances

The future development of optoelectronic devices will require an advanced control technology in electronic properties, for example by an external electric field (E_{field}). Here we demonstrate an approach that the heterostructure based on van der Waals (vdW) heterobilayer built by monolayer SnS_2 and PbI_2 has a well-controlled electronic properties with E_{field}. A type-II staggered-gap band alignment is achieved from the SnS_2/PbI_2 vdW heterostructure with which SnS_2 dominated the lowest energy holes as well as the lowest energy electrons are separated in PbI_2. The charge redistribution with an E_{field} is mainly on the surface of SnS_2 layer and PbI_2 and the numbers of polarized electrons on the monolayers display a linear evaluation with external E_{field}. The band structure under different E_{field} experiences not only a transition from semiconductor to metal but also conversions between type-I straddling-band alignment and type-II staggered-gap, which results in different spatial distribution of the lowest energy electrons and holes. Moreover, when the E_{field} is between -0.06 V Å^{-1} and -0.34 V Å^{-1}, the material manifests a varied direct bandgap which is more favor to optoelectronics and solar cell. Consequently, this vdW heterobilayer with well-controlled manner shows expectation for huge potential in optics and electronics.

1. Introduction

Ever since the successful manufacture of isolated graphene was reported,[1] two dimensional (2D) materials have become the subject of extensive research because of their superior optical and electronic properties. Hence, a broad family of 2D materials like graphene, such as BN,[2] transition metal dichalcogenides[3–5] and topological insulators[6–8] *etc.*, has been widely explored to solve that pristine graphene has a zero bandgap. Among them, recently, the SnS_2 2D films[9,10] have been poured unordinary attentions due to environmentally friendly and earth-abundant. For instance, it was reported that SnS_2 can be used as advance materials for photocatalytic,[11] field effect transistors[12] and anode in lithium batteries.[13] Meanwhile, previous studies on the lamellar semiconductor material of PbI_2 have reported that the freestanding single crystals PbI_2 could be prepared by a facile way.[14] Furthermore, PbI_2 has been demonstrated to be an attractive candidate of thin film transistors and can play the role of a precursor for the organ PbI_2 perovskites employed in highly efficient hybrid solar cells.[15–17] Accordingly, SnS_2 and PbI_2 have promising potential applications in optics and electronics.

For the sake of exploring materials in electronics, optoelectronics and photovoltaics devices, 2D materials can be used as building blocks restacked layer-by-layer in precisely chosen sequences yielding composites with unusual properties.[18,19] A brand new discipline is provided to tailor electronic and optical properties of 2D materials into new physics and device applications owing to their unique crystal properties. For instance, an enterprising and insightful approach has been recently exhibited that an atomically thin p–n diode can be manufactured by a vertically stacked heterobilayer between n-type MoS_2 and p-type WSe_2 slices,[20,21] which will not lead to doping problems.[22] Moreover, properties of vdW heterostructure would be more excellent than building blocks such as the SnS_2/MoS_2 vdW heterostructure exhibit an obvious photovoltaic effect and possess high mobility (27.6 cm^2 V^{-1} s^{-1}), high on/off ratio (>10^6) and high photoresponsivity (1.36 A W^{-1}), which is more outstanding than SnS_2 and MoS_2.[23] Thus, the vdW heterostructure with novel electronic and optoelectronic properties will reveal favorable properties and novel phenomena.

It is crucial to modify electronic properties of 2D materials for application in semiconductor devices and the two more effective ways are straining[24,25] and E_{field}.[26,27] In this article, we employed an external E_{field} to tunable the band structures because of reversibility and easy achievement. A quintessential example should be cited that the bandgap of bilayer graphene can be efficiently switched on *via* applications of electric field

[a]*College of Physics and Materials Science, Henan Normal University, Xinxiang, Henan 453007, China. E-mail: zhaoxu@htu.cn; xqdai@htu.cn*

[b]*School of Physics and Electronic Engineering, Zhengzhou Normal University, Zhengzhou, Henan 450044, China*

because the inversion symmetry of the structure was destroyed.[28,29] The fundamental bandgap of MoS_2, $MoSe_2$, $MoTe_2$ and WS_2 bilayer structures could be continuously modified with applied electric fields, eventually rendering them metallic.[30–32] Accordingly, utilization of E_{field} would lead to the realization of electronic properties engineering of the materials.

The bandgap of homobilayer SnS_2 could be continuously decreased with the electric field as well as different stacks[33] and a robust indirect band structure accompanied with the strength of increasing E_{field}. However, it is well known that the electron–hole recombination lifetime of the indirect bandgap semiconductor is longer than direct bandgap leading to lower the luminous efficiency, which is inappropriate for optoelectronic devices. Despite lots of researchers force on the modulation electronic properties of SnS_2 such as doping and strain,[10,12] there is no literature on SnS_2 with a direct bandgap.

In this work, we investigated the vdW heterostructure restacked by SnS_2 monolayer and PbI_2 monolayer to engineer an alternative type of advance optoelectronic material to realize any practical application of 2D vdW p–n junctions. The electronic properties have been systematically studied with external E_{field} by theoretical simulation and a well-behaved was found. The features make SnS_2/PbI_2 vdW heterobilayer a promising material for the advantage optoelectronic devices.

2. Theoretical methods

Our calculations were performed based on the density functional theory (DFT) in conjunction with the projector-augmented wave (PAW) potentials[34] as implemented in the Vienna *Ab initio* Simulation Package (VASP).[35,36] The exchange–correlation potentials was described through the Perdew–Burke–Ernzerhof (PBE) functional within the generalized gradient approximation (GGA) formalism.[37] The valence electron configurations for Sn, S, Pb and I were $4d^{10}5s^25p^2$, $3s^23p^4$, $5d^{10}6s^26p^2$ and $5s^25p^5$, respectively. The heterobilayer was built by $\sqrt{7} \times \sqrt{7}$ cells of SnS_2 and 2×2 cells of PbI_2. That a plane wave basis set with a cutoff energy of 480 eV and a $5 \times 5 \times 1$ *k*-points grids determined by a fine grid of gamma-centered Monkhorst–Pack method[38] in the Brillouin zone was found to give good converged results. The atomic structures were relaxed using conjugate gradient algorithm as implemented in the VASP code until the forces on all unconstrained atoms were smaller than 0.01 eV $Å^{-1}$. Moreover, a more precise method for the on-site Coulomb repulsion of Sn 4d and Pb 5d was considered in all calculations for the sake of more accurate bandgap. A PBE+U approach[39] was employed to treat exchange–correlation energy and the choice of $U = 9$ eV for Sn as well as 8.5 eV for Pb can reproduce the experimental bandgap of SnS_2 and PbI_2, respectively. Additionally, spin-orbital-coupling[40] was expected to be significant influence on the heavy atoms of lead (Pb), therefore it was considered in all calculation. A vacuum layer of 20 Å along *z* direction was constructed to eliminate the interaction with spurious replica images. The zero damping DFT-D3 method of Grimme[41] was used to account for long range vdW interaction between monolayer SnS_2 and PbI_2. All of structural figures and charge density drawings were produced by VESTA package.[42]

3. Results and discussion

The schematic illustration of monolayer SnS_2 and PbI_2 is displayed in Fig. 1. Primitive cells are plotted by a black line and a brief look for the vector of lattices is marked. After the total energy optimization, the lattice constants of monolayer SnS_2 and PbI_2 are respectively collected as 3.61 Å and 4.67 Å as exhibited in Table 1, that the agreements with previous studies are preeminent.[8,22,32] The properties of monolayer SnS_2 and PbI_2 are intensely sensitive to in-plane strains[43,44] so that the impact of strain on electronic structure should be reduced. To minimize the lattice mismatch between the stacking blocks, the supercell of this heterostructure is built by $\sqrt{7} \times \sqrt{7}$ of SnS_2 cells and 2×2 of PbI_2 cells, which the maximum mismatch for both SnS_2 and PbI_2 lattices is less than 2.3%.

The top and across views of the SnS_2/PbI_2 vdW heterostructure is presented in Fig. 1(c) and (d). The thicknesses of monolayers and the distance between SnS_2 and PbI_2 single-layer are respectively marked with *d* and *h* as displayed in Fig. 1(d). The optimized structural parameters and the binding energies are given in Table 1. After fully relaxed, the interlayer distance ($h = 3.49$ Å) is far greater than the sum of the covalent radii of I and S atom, indicating that the two building blocks are beyond the bonding range. To evaluate the stability, the binding energy (ΔE_b) of SnS_2/PbI_2 vdW heterobilayer was calculated and defined by,

$$\Delta E_b = (E_{SnS_2/PbI_2} - E_{SnS_2} - E_{PbI_2})/n, \quad (1)$$

where E_{SnS_2/PbI_2}, E_{SnS_2} and E_{PbI_2} represent total energy of the SnS_2/PbI_2 vdW heterostructure, SnS_2 monolayer and PbI_2 monolayer, respectively. Meanwhile, $[SnS_2]$ unit cells in the superlattice are marked as *n* which equals to seven in this article. By this definition, a negative ΔE_b is indicative of that the heterostructure is stable.

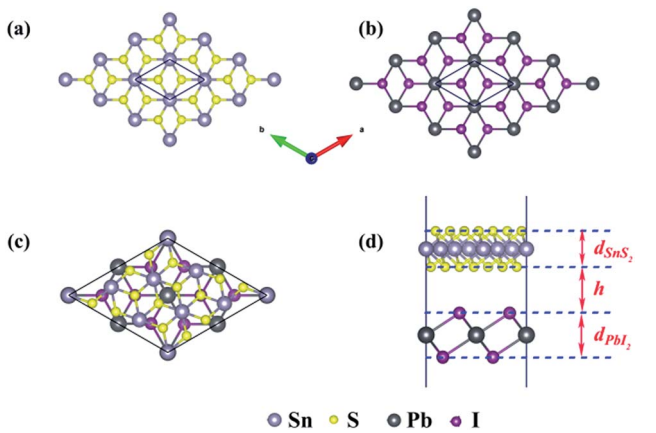

Fig. 1 Schematic of the monolayers and the SnS_2/PbI_2 vdW heterobilayer. Top view of (a) SnS_2 and (b) PbI_2 monolayer. The top (c) and side view (d) of the heterobilayer. Silvery, yellow, dark grey and purple spheres represent Sn, S, Pb and I atoms, respectively.

Table 1 The lattice constants of SnS_2 monolayer, PbI_2 monolayer and the SnS_2/PbI_2 vdW heterostructure, respectively

		a (Å)	d (Å)	h (Å)
SnS_2 monolayer		3.61	2.98	
PbI_2 monolayer		4.67	3.72	
The heterostructure	SnS_2 monolayer	9.45	3.03	3.49
	PbI_2 monolayer		3.68	

The binding energy of SnS_2 and PbI_2 vdW heterobilayer is −0.124 eV per SnS_2 unit, which is indicative of a rather weak but stable interaction between the layers. This could be just more evidence for that the interaction between SnS_2 monolayer and PbI_2 monolayer is mainly forced through van der Waals interactions because ΔE_b has the same order of magnitude as the other vdW substances, for example, graphite ($\Delta E_b = -0.10$ eV per C atom),[45] bilayer SnS_2 ($\Delta E_b = -0.05$ eV per SnS_2 unit),[33] the MoS_2/PbI_2 heterostructure ($\Delta E_b = -0.234$ eV per MoS_2 unit)[46] and black phosphorus/MoS_2 heterobilayer ($\Delta E_b = -0.108$ eV per MoS_2 unit).[47]

We calculate the band structures of monolayer SnS_2 (Fig. 2(a)) and PbI_2 (Fig. 2(b)) as well as the SnS_2 and PbI_2 vdW heterostructure (Fig. 2(c)) to obtain the electronic properties based on PBE+U approach. For SnS_2 monolayer, the fundamental band structure is an indirect bandgap of about 2.22 eV that the valance band maximum (VBM) is extremely close to Γ point and the conduction band minimum (CBM) lies at M which is close to the reported values.[12,48] Additionally, the smallest gap of PbI_2 monolayer appears between the CBM at Γ and the VBM which medially lies between K and Γ that the agreements with previous studies are preeminent.[43]

In Fig. 2(c), we present the projected band structure of the SnS_2 and PbI_2 in the vdW heterobilayer that the blue lines represent of SnS_2 monolayer and the red lines are for PbI_2, respectively. As can be seen in Fig. 2(c), the SnS_2 monolayer and PbI_2 monolayer compose a type-II staggered-gap band alignment that the CBM is contributed by SnS_2 whereas the VBM by PbI_2 with a bandgap of about 1.98 eV. In consequence, the Fermi level shifts to the CBM of SnS_2 and VBM of PbI_2 after they compose the heterobilayer. It can be looking forward that the photoelectric property will be improved distinctively because the lowest energy electron–hole pairs can separate in real space. Compared with the band structure, band alignment of heterostructure are even more important in material and device design. Meanwhile, the work function ($\Phi = E_{Van} - E_F$, where the E_{Van} is the vacuum level and the E_F is the Fermi level, respectively) and band alignment is shown in Fig. 2(d). It is indicated that a type-II band alignment of vdW heterostructure is formed at the SnS_2/PbI_2 interface which will spontaneously separate the free electrons and holes, enabling the high efficiency optoelectronics and solar energy conversion.

To shed more lights on the nature of the charge transfer between the SnS_2 and PbI_2 layer, the averaged difference electron density of the heterostructure along the z direction was calculated by the formula

$$\Delta\rho = \int \rho_{SnS_2/PbI_2}(x,y,z)\mathrm{d}x\mathrm{d}y - \int \rho_{SnS_2}(x,y,z)\mathrm{d}x\mathrm{d}y - \int \rho_{PbI_2}(x,y,z)\mathrm{d}x\mathrm{d}y, \quad (2)$$

where the $\int \rho_{SnS_2/PbI_2}(x,y,z)\mathrm{d}x\mathrm{d}y$, $\int \rho_{SnS_2}(x,y,z)\mathrm{d}x\mathrm{d}y$ and $\int \rho_{PbI_2}(x,y,z)\mathrm{d}x\mathrm{d}y$ are the charge density at the (x, y, z) point in the SnS_2/PbI_2 bilayer, SnS_2 and PbI_2 monolayer, respectively. Accordingly, a positive value means electron accumulation and negative for depletion. The result is exhibited in Fig. 3(a), that the vertical blue short dash line means the intermediate position for the interface of the building blocks as well as the positions of Sn, S, Pb and I atomic layers are marked as purple, dark grey, yellow and silvery and short dot lines, respectively. As a result of the interlayer coupling effect, there is an obvious charge accumulation region as the SnS_2/PbI_2 heterointerface. Moreover, there is a small amount of electrons (about $0.453 \times 10^{-3}|e|$) transferring from PbI_2 to SnS_2 layer, further indicating a weak interlayer coupling between SnS_2 layer and PbI_2 layer. Furthermore, a built-in electrical field formed intrinsic spontaneous of electric polarization is expected and directed from PbI_2 to SnS_2.

It is crucial to modify electronic properties of 2D materials for application in semiconductor devices so that an external E_{field} perpendicular to the heterobilayer is employed. The

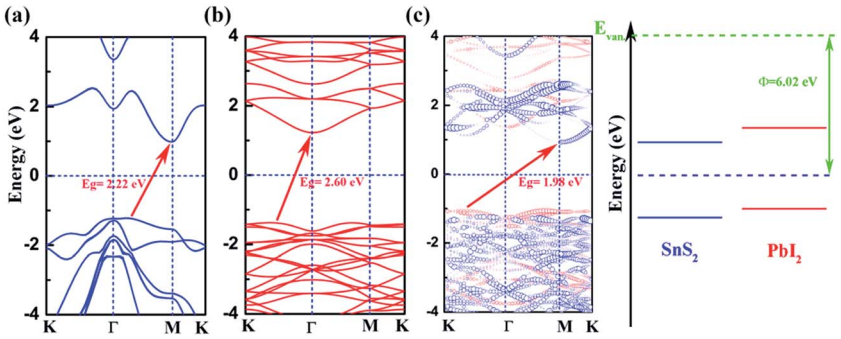

Fig. 2 Electronic band structures of (a) PbI_2, (b) SnS_2. (c) The projected band structure as well as schematic of band alignment of SnS_2/PbI_2 vdW heterostructure (blue and red lines respectively represent for SnS_2 and PbI_2 layer). The Fermi level is set to zero and marked by horizontal blue dotted line. The vacuum level is taken as a reference marked by green horizontal dash.

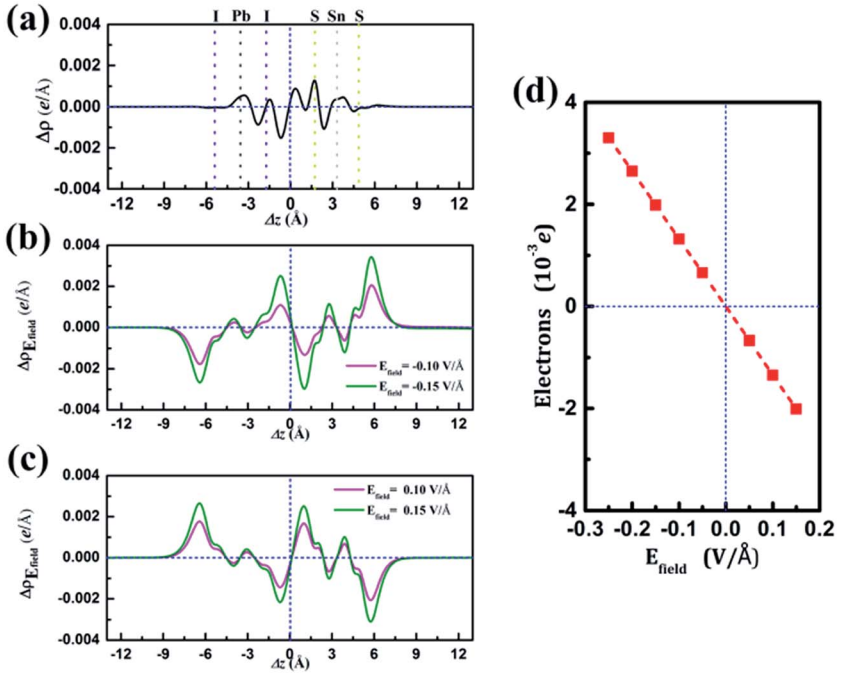

Fig. 3 (a) The averaged difference electron density of SnS_2/PbI_2 heterostructure along z direction. (b) and (c) The integrated charge density difference of the heterobilayer under different external E_{field}. (d) The transferred electrons as a function of E_{field}. The positive values of electrons in (d) indicate a transferred direction from SnS_2 to PbI_2 layer.

positive direction of E_{field} is set from PbI_2 layer to SnS_2 layer. To evaluate the influences of E_{field} modulating on the electronic properties of the heterostructure, the integrated charge density difference with E_{field} along z direction was employed and determined as,

$$\Delta\rho_{E_{field}} = \int \rho^{E_{field}\neq 0}_{SnS_2/PbI_2}(x,y,z)\mathrm{d}x\mathrm{d}y - \int \rho^{E_{field}=0}_{SnS_2/PbI_2}(x,y,z)\mathrm{d}x\mathrm{d}y, \quad (3)$$

where $\int \rho^{E_{field}\neq 0}_{SnS_2/PbI_2}(x,y,z)\mathrm{d}x\mathrm{d}y$ and $\int \rho^{E_{field}=0}_{SnS_2/PbI_2}(x,y,z)\mathrm{d}x\mathrm{d}y$ are the charge density at (x, y, z) point of SnS_2/PbI_2 heterostructure with and without E_{field}. The results are displayed in Fig. 3(b) and (c). It is obvious that the charge redistribution is mainly on the surface of SnS_2 and PbI_2 layers. The positive charges (holes) tend to transfer from SnS_2 layer to PbI_2 layer and negative charges (electrons) transfer from PbI_2 layer to SnS_2 layer in the case of a negative E_{field} as well as positive E_{field} lead to the opposite direction of charge and hole transfers. Additionally, the amount of transferring electrons depends on the strength of the applied E_{field}.

To shed more lights on the charge redistribution with E_{field}, the numbers of polarized electrons on the building blocks were obtained through integrating the charge density from the vacuum layer to the intermediate position of the interface of the monolayers as exhibited in Fig. 3(d). The positive value means the electron transfers from SnS_2 layer to PbI_2 layer. The numbers of polarized electrons on the building blocks display a linear evaluation with external E_{field} and a transitional on the direction depends on the direction of E_{field} is found, which is identical with above analyses. The accumulation of electrons (holes) will lead to the Fermi level down (up)-shifted of SnS_2 and PbI_2 monolayer which thereby bring about modulation of the band structure. More charge transfer between SnS_2 and PbI_2 layer heralds a stronger interlayer interaction, indicating the shifts of band edges.

This could be graphically explained in Fig. 4(a), which manifests the evolution of the bandgap of SnS_2/PbI_2 heterostructure as a function of applied E_{field}. The bandgap is continuously tuned under the E_{field}, eventually achieving a mutation from semiconductor to metal at critical E_{field}. The bandgap varies linearly with E_{field} indicating a giant Stark effect.[49] It is almost lineally reduced with the strength of E_{field} reducing to zero bandgap at the E_{field} of about 0.28 V Å^{-1} when a forward voltage is applied. For a negative E_{field}, the bandgap firstly increases reaching up to 2.19 eV which appears at an E_{field} of about −0.03 V Å^{-1}. The encouragement of bandgap is due to the presence of intrinsic spontaneous of electric polarization which is opposite to the E_{field} and has a superimposing effect on it. Further increases in strength of negative E_{field} ($|E_{field}| > 0.06$ V Å^{-1}) lead to linearly decreases in bandgap and the heterobilayer turns metallic at about −0.34 V Å^{-1}.

To gain further insight, band edges dominated by SnS_2 and PbI_2 under various E_{field} are calculated and displayed in Fig. 4(b). The CBM and VBM of SnS_2(PbI_2) of the vdW heterobilayer are denoted by $CBM_{SnS_2(PbI_2)}$ and $VBM_{SnS_2(PbI_2)}$, respectively. Both the CBM and VBM of SnS_2 decrease linearly with E_{field} while the CBM and VBM of PbI_2 manifest a linear increase. The E_{field} exerts litter influence on the respective bandgaps of SnS_2 and PbI_2. The bandgap of SnS_2/PbI_2 heterostructure gives the same variation trend with Fig. 4(a). Additionally, the band alignment conversion from type-II to type-I heterostructure

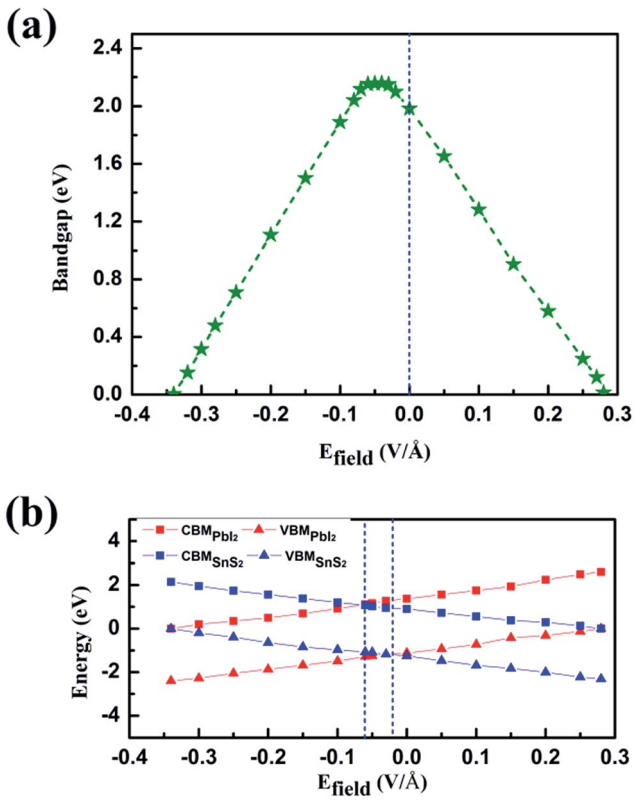

Fig. 4 (a) Bandgap variation with applied E_{field} of the SnS_2/PbI_2 vdW heterostructure. (b) Evolution of the band edges in SnS_2/PbI_2 heterostructure as a function of the E_{field}. $CBM_{SnS_2(PbI_2)}$ and $VBM_{SnS_2(PbI_2)}$ are the CBM and VBM of $SnS_2(PbI_2)$ in the vdW heterobilayer.

separated by the E_{field} about -0.03 V Å^{-1} and then from type-I to type-II by about -0.06 V Å^{-1}, resulting in different spatial distribution of the lowest energy electrons and holes.

Energy dispersion with and without E_{field} is displayed in Fig. 5(a)–(d), respectively. With an E_{field} of -0.15 V Å^{-1}, the heterobilayer manifests a direct bandgap that both the CBM and VBM are located at Γ point. The direct bandgap semiconductor has a less electron–hole recombination lifetime with a high luminous efficiency which is overwhelmingly suitable for optoelectronic devices. The location of CBM changes from Γ to M point in the Brillouin zone but the VBM is still at Γ point leading to an indirect bandgap in the case of $E_{field} = -0.05$ V Å^{-1} as shown in Fig. 5(b). When an E_{field} of 0.15 V Å^{-1} is added to the vdW heterostructure, the band structure manifests an indirect bandgap that the CBM located at M point and VBM between K to Γ point (Fig. 5(d)).

The partial charge densities of the heterostructure from CBM and VBM with different E_{field} are calculated and summarized in Fig. 5. When the SnS_2/PbI_2 vdW heterobilayer subjected to a negative E_{field} of -0.15 V Å^{-1}, it is clearly shown that the partial charge density from CBM is dominated by Pb atoms and the VBM comes mainly from the SnS_2 layer, as shown in Fig. 5(a). That is to say, the staggered-gap band alignment be suggestive of a type-II heterojunction. Both the CBM and VBM of the heterobilayer, when the heterobilayer suffered by an E_{field} of -0.05 V Å^{-1}, are all straddled by SnS_2 layer (Fig. 5(b)) indicating a type-I heterojunction. When the heterobilayer suffered by the E_{field} of 0 V Å^{-1} or 0.15 V Å^{-1}, the partial charge density from CBM is dominated by Sn atoms and the VBM by I atomical layer displayed in Fig. 5(c) and (d), respectively. Thus, a type-II

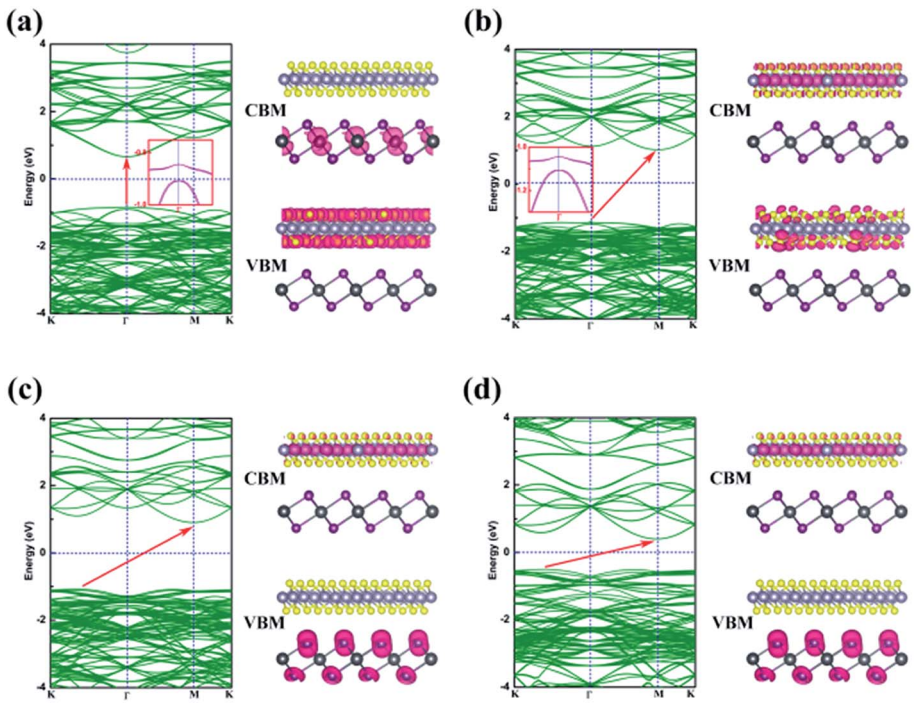

Fig. 5 Band structures and partial charge densities plot for the CBM and VBM of the SnS_2/PbI_2 vdW heterostructure with and without E_{field}. (a) $E_{field} = -0.15$ V Å^{-1}, (b) $E_{field} = -0.05$ V Å^{-1}, (c) $E_{field} = 0$ V Å^{-1}, and (d) $E_{field} = 0.15$ V Å^{-1}. All isosurfaces of this text are set to 0.004 e Å^{-3}.

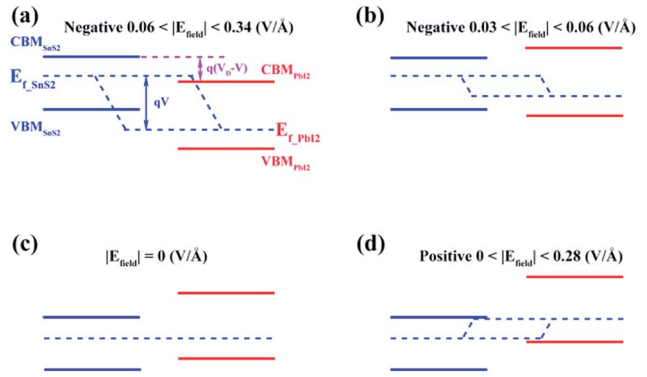

Fig. 6 Band alignments of the SnS_2/PbI_2 vdW heterobilayer under different E_{field}.

staggered-gap band alignment is obtained with an alternation of CBM and VBM between the monolayer SnS_2 and PbI_2. Briefly, the band structures can be effectively modulated by an external electric field.

Similar evidence also comes from the band alignment of SnS_2/PbI_2 heterostructure under various E_{field}, as seen in Fig. 6. The $E_{f\text{-}SnS_2(PbI_2)}$ indicate the quasi-Fermi level of $SnS_2(PbI_2)$ in the vdW heterobilayer. V_D denote the conduction band offset in the SnS_2/PbI_2 heterostructure without an E_{field} as well as $V = E_{field} \times d$ is the external electric potential, which leads to the divergence of the quasi-Fermi levels. The interlayer distance is marked with d, which is a constant in this case. When the SnS_2/PbI_2 vdW heterostructure subjected to a negative E_{field}, the bandgap varies with E_{field} in the following function:

$$E_g = E_{g(SnS_2)} - e(V_D - V) = E_{g(SnS_2)} - eV_D + eE_{field} \times d. \quad (4)$$

The maximum bandgap is obtained when the E_{field} reaches to -0.03V Å^{-1}. Even the electric field increasing to -0.06V Å^{-1}, both the CBM and VBM of the heterobilayer are all straddled by SnS_2 layer. So, bandgap can be obtained as,

$$E_g = E_{g(SnS_2)} \approx 2.19 \text{ eV}.$$

Under circumstances of E_{field} greater than 0.06 V Å^{-1} along the negative direction, the bandgap varies as the function:

$$E_g = E_{g(SnS_2)} - e(E_{field} - 0.06)d.$$

The linear evaluations of bandgap with the strength of E_{field} are obtained as the $E_{g(SnS_2)}$ and e is constant. Meanwhile, the varied relationship between bandgap and E_{field} shares the same evidence of the giant Stark effect.

4. Conclusions

In summary, a vdW heterostructure of SnS_2 and PbI_2 has been theoretically simulated and the heterobilayer has a well-behaved electronic property under an external E_{field}. A type-II staggered-gap band alignment is constituted which the spatial separation of the lowest energy electron–hole pairs can be actualized. When suffered under an external E_{field}, the charge redistribution is mainly on the surface of SnS_2 and PbI_2 layers and the numbers of polarized electrons on the building blocks display a linear evaluation with external E_{field}. Meanwhile, the transitional direction depends on the direction of E_{field}. The external E_{field} not only influences the band structure which changes from semiconductor to metal but also forces on band alignment which experiences a conversion between type-I straddling-band alignment type-II broken-gap, leading to a different spatial distribution of the lowest energy electrons and holes. A direct bandgap of the heterobilayer is found among -0.06 V Å^{-1} and -0.34 V Å^{-1}. This work could bring forward a new perspective on advantage optoelectronics devices with a well-E_{field}-controlled manner by using SnS_2/PbI_2 vdW heterostructure.

Acknowledgements

This work was financially supported by the National Natural Science Foundation of China (Grant no. 61674053, 11504092 and 11504334), the Natural Science Foundation of Henan Province (Grant No. 162300410325) and by the High Performance Computing Center of Henan Normal University.

References

1 K. S. Novoselov, A. K. Geim, S. V. Morozov, D. Jiang, Y. Zhang, S. V. Dubonos and A. A. Firsov, *Science*, 2007, **306**, 666–669.
2 L. Wirtz, A. Marini and A. Rubio, *Phys. Rev. Lett.*, 2005, **96**, 126104.
3 Q. Wang, K. Kalantar-Zadeh, A. Kis, J. Coleman and M. S. Strano, *Nat. Nanotechnol.*, 2012, **7**, 699–712.
4 W. Li, T. Wang, X. Dai, X. Wang, C. Zhai, Y. Ma and S. Chang, *Solid State Commun.*, 2016, **250**, 9–13.
5 H. Liu, H. Zheng, F. Yang, L. Jiao, J. Chen, W. Ho, C. Gao, J. Jia and M. Xie, *ACS Nano*, 2015, **9**, 6619–6625.
6 S. Zhang, B. Bernevig and T. Hughes, *Science*, 2007, **314**, 1757–1761.
7 X. Zhao, X. Dai, B. Zhao, N. Wang and Y. Ji, *J. Phys.: Condens. Matter*, 2013, **25**, 265005.
8 B. Li, X. Guo, W. Ho and M. Xie, *Appl. Phys. Lett.*, 2015, **107**, 081604.
9 R. RMitchell, Y. Fujiki and Y. Ishizawa, *Nature*, 1974, **247**, 537–538.
10 C. Xia, X. Zhao, Y. Peng, H. Zhang, S. Wei and Y. Jia, *Superlattices Microstruct.*, 2015, **85**, 664–671.
11 Y. Sun, H. Cheng, S. Gao, Z. Sun, Q. Liu, Q. Liu, F. Lei, T. Yao, J. He, S. Wei and Y. Xie, *Angew. Chem.*, 2012, **51**, 8727–8731.
12 C. Xia, Y. Peng, H. Zhang, T. Wang, S. Wei and Y. Jia, *Phys. Chem. Chem. Phys.*, 2014, **16**, 19674–19680.
13 M. He, L. Yuan and Y. Huang, *RSC Adv.*, 2013, **3**, 3374–3383.
14 X. Zhu, Y. Wang, H. Sun, D. Yang, X. Gao and H. Tian, *Mater. Lett.*, 2016, **180**, 59–62.

15 H. Wang, X. Hu and H. Chen, *RSC Adv.*, 2015, **5**, 30192–30196.
16 A. Kojima, K. Teshima, Y. Shirai and T. Miyasaka, *J. Am. Chem. Soc.*, 2009, **131**, 6050.
17 A. Abate, M. Planells, D. J. Hollman, V. Barthi, S. Chand, H. J. Snaith and N. Robertson, *Phys. Chem. Chem. Phys.*, 2014, **17**, 2335.
18 A. K. Geim and I. V. Grigorieva, *Nature*, 2013, **499**, 419.
19 Q. Sun, Y. Dai, Y. Ma, N. Yin, W. Wei, L. Yu and B. Huang, *2D Mater.*, 2016, **3**, 035017.
20 R. Cheng, D. Li, H. Zhou, C. Wang, A. Yin, S. Jiang, Y. Liu, Y. Chen, Y. Huang and X. Duan, *Nano Lett.*, 2014, **14**, 5590–5597.
21 N. Huo, J. Yang, L. Huang, Z. Wei, S. Li, Z. Wei and J. Li, *Small*, 2015, **11**, 5430–5438.
22 M. M. Furchi, A. A. Zechmeister, F. Hoeller and S. Wachter, *IEEE J. Sel. Top. Quantum Electron.*, 2015, **14**, 8.
23 B. Li, L. Huang, M. Zhong, Y. Li, Y. Wang, J. Li and Z. Wei, *Adv. Electron. Mater.*, 2016, **2**, 1600298.
24 L. Huang, Y. Li, Z. Wei and J. Li, *Sci. Rep.*, 2015, **5**, 16448.
25 W. Xiong, C. Xia, X. Zhao, W. Wang and Y. Jia, *Carbon*, 2016, **109**, 737–746.
26 W. Li, T. Wang, X. Dai, Y. Ma and Y. Tang, *J. Alloys Compd.*, 2017, **705**, 486–491.
27 C. Xai, B. Xue, T. Wang, Y. Peng and Y. Jia, *Appl. Phys. Lett.*, 2015, **107**, 193107.
28 E. Mccann, *Phys. Rev. B: Condens. Matter Mater. Phys.*, 2006, **74**, 161403.
29 M. K. Madito, N. Manyala, A. Bello, J. K. Dangbegnon, T. M. Masikhwa and D. Y. Momodu, *RSC Adv.*, 2016, **6**, 28370–28378.
30 A. Ramasubramaniam, D. Naveh and E. Towe, *Phys. Rev. B: Condens. Matter Mater. Phys.*, 2011, **84**, 203239–203247.
31 Z. Huang, C. He, X. Qi, H. Yang, W. Liu, X. Wei, X. Peng and J. Zhong, *J. Phys. D: Appl. Phys.*, 2014, **47**, 75301–75306.
32 L. Huang and J. Li, *Appl. Phys. Lett.*, 2016, **108**, 147.
33 P. Guo, T. Wang, C. Xia and Y. Jia, *Appl. Phys. A*, 2016, **122**, 1–7.
34 G. Kresse and D. Joubert, *Phys. Rev. B: Condens. Matter Mater. Phys.*, 1999, **59**, 1758–1775.
35 G. Kresse and J. Furthmüller, *Comput. Mater. Sci.*, 1996, **6**, 15–50.
36 P. E. Blöchl, *Phys. Rev. B: Condens. Matter Mater. Phys.*, 1994, **50**, 17953–17979.
37 J. P. Perdew, K. Burke and M. Ernzerhof, *Phys. Rev. Lett.*, 1996, **77**, 3865.
38 H. J. Monkhorst and J. D. Pack, *Phys. Rev. B: Condens. Matter Mater. Phys.*, 1976, **13**, 5188.
39 S. Dudarev, G. Botton, S. Savrasov, C. Humphreys and A. Sutton, *Phys. Rev. B: Condens. Matter Mater. Phys.*, 1998, **57**, 1505–1509.
40 A. Bermudez, F. Jelezko, M. B. Plenio and A. Retzker, *Phys. Rev. Lett.*, 2011, **107**, 3745.
41 S. Grimme, J. Antony, S. Ehrlich and H. Krieg, *J. Chem. Phys.*, 2010, **132**, 154104–154119.
42 K. Momma and F. Izumi, *J. Mineral. Petrol. Sci.*, 2010, **39**, 136–145.
43 M. Zhou, W. Duan, Y. Chen and A. J. Du, *Nanoscale*, 2015, **7**, 15168–15174.
44 B. Ram, A. Manjanath and A. K. Singh, *2D Mater.*, 2016, **3**, 015009.
45 G. Graziano, J. Klimeš, F. Fernandez-Alonso and A. Michaelides, *J. Phys.: Condens. Matter*, 2012, **24**, 424216.
46 Y. Ma, X. Zhao, T. Wang, W. Li, X. Wang, S. Chang, Y. Li, M. Zhao and X. Dai, *Phys. Chem. Chem. Phys.*, 2016, **18**, 28466.
47 L. Huang, N. Huo, Y. Li, H. Chen, J. Yang, Z. Wei and J. Li, *J. Phys. Chem. Lett.*, 2015, **6**, 2483.
48 L. A. Burton, T. J. Whittles, D. Hesp, W. M. Linhart, J. M. Skelton, B. Hou, R. F. Webster, G. O'Dowd, C. Reece, D. Cherns, D. J. Fermin, T. D. Veal, V. R. Dhanak and A. Walsh, *J. Mater. Chem. A*, 2016, **4**, 1312.
49 F. Zheng, Z. Liu, J. Wu, W. Duan and B. Gu, *Phys. Rev. B: Condens. Matter Mater. Phys.*, 2008, **78**, 085423.